Lloyd's formula in multiple-scattering calculations with finite temperature

2005 J. Phys.: Condens. Matter 17 5367

(http://iopscience.iop.org/0953-8984/17/35/005)

INSTITUTE OF PHYSICS PUBLISHING JOURNAL OF PHYSICS: CONDENSED MATTER

J. Phys.: Condens. Matter **17** (2005) 5367–5379 doi:10.1088/0953-8984/17/35/005

Lloyd's formula in multiple-scattering calculations with finite temperature

Rudolf Zeller

Institut für Festkörperforschung, Forschungszentrum Jülich GmbH, D-52425 Jülich, Germany

E-mail: Ru.Zeller@fz-juelich.de

Received 7 June 2005, in final form 19 July 2005
Published 19 August 2005
Online at stacks.iop.org/JPhysCM/17/5367

Abstract

Lloyd's formula is an elegant tool to calculate the number of states directly from the imaginary part of the logarithm of the Korringa–Kohn–Rostoker (KKR) determinant. It is shown how this formula can be used at finite electronic temperatures and how the difficult problem to determine the physically significant correct phase of the complex logarithm can be circumvented by working with the single-valued real part of the logarithm. The approach is based on contour integrations in the complex energy plane and exploits the analytical properties of the KKR Green function and the Fermi–Dirac function. It leads to rather accurate results, which is illustrated by a local-density functional calculation of the temperature dependence of the intrinsic Fermi level in zinc-blende GaN.

1. Introduction

Lloyd's formula [1, 2] for the integrated density of states is an important concept in the Korringa–Kohn–Rostoker (KKR) multiple-scattering method [3, 4]. Lloyd's formula provides an analytical integration over energy and space and directly gives the total number of states as function of energy. The angular-momentum convergence of Lloyd's formula is fast, since it is directly related to the decrease of the phase shifts which usually rapidly decrease for the higher angular-momentum channels. Nevertheless, Lloyd's formula is not often used in electronic structure calculations and its application is mainly restricted to calculations within the coherent-potential approximation and for impurities, for which it improves calculated total energies, for instance impurity solution energies, in a spectacular manner [5]. One difficult problem for the numerical application of Lloyd's formula is the determination of the correct phase of the multivalued complex logarithm of the KKR determinant. The calculated value of the KKR determinant at the local energy E alone does not contain the information about the correct branch of the logarithm. The branch is necessary to determine the number of states from the correct multiple of π of the phase and can only be found if the global behaviour of the KKR determinant for all energies below E is taken into account.

It is the aim of this paper to present a method for a reliable and accurate calculation of Lloyd's formula and to show how it can be used together with Fermi–Dirac statistics in finite-temperature electronic-structure calculations. The method is based on contour integrations in the complex energy plane and exploits the analytical properties of the KKR Green function and the Fermi–Dirac function. For periodic crystals the method conveniently applies the concept of a repulsive reference system, which is used in the tight-binding (screened) KKR method and consists of an infinite array of repulsive muffin-tin potentials [6]. It will be discussed why the repulsive reference system is better suited than the usually applied free-space reference system and it will be shown that the results are accurate enough to determine the effect of the Fermi–Dirac statistics on the temperature dependence of the intrinsic Fermi level of semiconductors. This will be illustrated by a local-density-functional calculation for GaN in its zinc-blende structure.

The outline of the paper is as follows. First the basic equations for Lloyd's formula in the KKR Green-function method and the numerical details of the calculations are described. After this the effects of angular-momentum convergence, Brillouin-zone sampling and real-space construction of the structure constants of the reference system are investigated. Then it is shown how Lloyd's formula can be applied together with finite temperatures. Finally, the approach is presented, which circumvents the phase problem and is accurate enough for the determination of the temperature dependence of the intrinsic Fermi level.

2. Lloyd's formula in the KKR Green-function method

The number of occupied electronic states as function of chemical potential μ and temperature T is given by

$$N_{\mathrm{e}}(\mu, T) = -\frac{1}{\pi}\,\mathrm{Im}\int_{-\infty}^{\infty} \mathrm{d}E\; f(E, \mu, T)\,\mathrm{Tr}\,G(E), \tag{1}$$

where $f(E, \mu, T) = (1 + \exp(\beta(E - \mu)))^{-1}$ is the Fermi–Dirac function with $\beta^{-1} = kT$ and $\mathrm{Tr}\,G(E)$ is the trace of the single-particle Green function. The multiple-scattering representation of the Green function can be written as

$$G(\mathbf{r} + \mathbf{R}^n, \mathbf{r}' + \mathbf{R}^{n'}; E) = \delta_{nn'} \sum_L R^n_L(\mathbf{r}_<; E) S^n_L(\mathbf{r}_>; E) + \sum_{LL'} R^n_L(\mathbf{r}; E) G^{nn'}_{LL'}(E) R^{n'}_{L'}(\mathbf{r}'; E) \tag{2}$$

in the notation of [7], where $\mathbf{r}$ and $\mathbf{r}'$ are site-centred coordinates and $\mathbf{R}^n$ and $\mathbf{R}^{n'}$ denote the scattering sites. The vectors $\mathbf{r}_<$ and $\mathbf{r}_>$ stand for $\mathbf{r}$ or $\mathbf{r}'$ with smaller or larger length. The Green-function matrix elements $G^{nn'}_{LL'}(E)$ can be obtained by an algebraic Dyson equation [8] from the Green-function matrix elements $G^{r,nn'}_{LL'}(E)$ of a reference system. For $r > r^n_{\mathrm{s}}$, where r^n_{s} is the radius of the sphere circumscribed around the Wigner–Seitz or Voronoi cell at site $\mathbf{R}^n$, the single-scattering solutions $S^n_L(\mathbf{r}; E)$ and $R^n_L(\mathbf{r}; E)$ fulfil the boundary conditions

$$S^n_L(\mathbf{r}; E) = -\mathrm{i}\sqrt{E} h^{(1)}_l(r\sqrt{E}) Y_L(\hat{\mathbf{r}}) \tag{3}$$

$$R^n_L(\mathbf{r}; E) = j_l(r\sqrt{E}) Y_L(\hat{\mathbf{r}}) - \mathrm{i}\sqrt{E} \sum_{L'} h^{(1)}_{l'}(r\sqrt{E}) Y_{L'}(\hat{\mathbf{r}}) t^n_{L'L}(E) \tag{4}$$

with $t^n_{LL'}(E)$ defined as

$$t^n_{LL'}(E) = \int_n \mathrm{d}\mathbf{r}\, j_l(r\sqrt{E}) Y_L(\hat{\mathbf{r}}) V^n(\mathbf{r}) R^n_{L'}(\mathbf{r}, E). \tag{5}$$

Here the integral is over cell n and j_l and $h^{(1)}_l$ denote spherical Bessel and Hankel functions and Y_L spherical harmonics with a combined index $L = lm$.

In numerical calculations the sums in (2) must be truncated to a finite number of angular momenta L. This prevents the correct normalization of the multiple-scattering Green function and represents a fundamental problem. This problem has been recognized in the past [9–14] and it particularly affects insulators and semiconductors, where the position of the Fermi level cannot be determined in this way. In these materials only an exact normalization guarantees that the Fermi level falls into the bandgap. A small, even tiny error in the normalization always means that the calculated Fermi level is physically incorrectly placed either in the valence or in the conduction band. In metals the error is much less pronounced, since due to the partial occupation of states the Fermi level is only slightly changed by an incorrect normalization and does not occur in a principally wrong position. But also in metals serious errors can occur, for instance, in the normalization of semicore states. The wrong normalization of these states is counterbalanced by a Fermi level shift, which despite its smallness can lead to a large error of the total energy.

A solution for this problem can be obtained by rewriting (1) as

$$N_{\mathrm{e}}(\mu, T) = -\mathrm{Im} \int_{-\infty}^{\infty} \mathrm{d}E\, N(E) \frac{\mathrm{d}}{\mathrm{d}E} f(E, \mu, T) \tag{6}$$

and by using Lloyd's formula for $N(E) = -\frac{1}{\pi} \int^{E} \mathrm{d}E' \,\mathrm{Tr}\, G(E')$. Note that here $N(E)$ is used as a complex quantity and that its imaginary part gives the usual integrated density of states. The appropriate form of Lloyd's formula [1, 15], valid for complex energies and full potentials, has been given by Drittler *et al* [5, 16, 17] in the form

$$N(E) = N^{r}(E) + \frac{1}{\pi} \sum_{n} \ln \det |\Delta\alpha^{n}_{LL'}(E)| - \frac{1}{\pi} \ln \det |\delta^{nn'}_{LL'} - G^{r,nn'}_{LL'}(E) \Delta t^{n'}_{LL'}(E)|, \tag{7}$$

where the sum is over the cells and the Δt and $\Delta\alpha$ matrices are changes with respect to the reference system. The KKR determinant $\det |1 - G^{r} \Delta t|$ is over combined angular-momentum and cell indices, whereas the determinant $\det |\Delta\alpha|$ is over angular-momentum indices alone. For periodic crystals with an infinite number of atoms, (7) cannot be used directly because it gives an infinite result. Then $N(E)$ defined per unit cell as

$$\begin{aligned} N(E) = N^{r}(E) &+ \frac{1}{\pi} \sum_{\nu} \ln \det |\Delta\alpha^{\nu}_{LL'}(E)| \\ &- \frac{1}{\pi V_{\mathrm{BZ}}} \int_{\mathrm{BZ}} \mathrm{d}\mathbf{k} \ln \det |\delta^{\nu\nu'}_{LL'} - G^{r,\nu\nu'}_{LL'}(\mathbf{k}, E) \Delta t^{\nu'}_{LL'}(E)| \end{aligned} \tag{8}$$

can be used, where the integral is over the Brillouin-zone and where the sum over ν and the site indices ν, ν' in the KKR determinant are restricted to the basis sites within the unit cell. In (7) and (8) the quantity $N^{r}(E)$ is the 'integrated density of states' of the reference system and $G^{r,nn'}_{LL'}(E)$ and $G^{r,\nu\nu'}_{LL'}(\mathbf{k}, E)$ are the Green-function matrix elements of the reference system and their lattice Fourier transforms. The matrix $\Delta\alpha$ describes the different behaviour of the single-scattering solutions R^{n}_{L} and $R^{r,n}_{L}$ at the origin

$$R^{n}_{L}(\mathbf{r}, E) = \sum_{L'} R^{r,n}_{L'}(\mathbf{r}, E) \Delta\alpha^{n}_{L'L}(E) \qquad \text{for } r \to 0 \tag{9}$$

and can be calculated by

$$\Delta\alpha^{n}_{LL'}(E) = \delta_{LL'} + \int_{n} \mathrm{d}\mathbf{r} S^{r,n}_{L}(\mathbf{r}, E) \Delta V^{n}(\mathbf{r}) R^{n}_{L'}(\mathbf{r}, E), \tag{10}$$

where $\Delta V(\mathbf{r}) = V(\mathbf{r}) - V^{r}(\mathbf{r})$ is the difference of potentials and $S^{r,n}_{L}$ and $R^{r,n}_{L}$ are the single-scattering solutions of the reference system satisfying boundary conditions as in (3) and (4).

The problem with the evaluation of the total number of states is a characteristic feature of the Green-function version of the KKR method. In the traditional KKR method the eigenfunctions of the genuinely infinite-dimensional KKR matrix are calculated by truncating this matrix to the subspace of low angular momenta $l \leqslant l_{\max}$ and by normalizing the eigenfunctions in this subspace [18]. In this way the correct number of states is obtained, although a proper normalization would require all angular momenta $l < \infty$. In a sense, by restriction to a subspace, the weight of the momenta $l > l_{\max}$ is transferred to the lower l values $l \leqslant l_{\max}$. Basically similar subspace procedures are followed in any finite-basis-set method.

3. Details of the numerical calculations

The calculations were performed by the Jülich full-potential KKR program [8], where the form of the Wigner–Seitz cells is described by shape functions $\Theta(\mathbf{r})$, which are expanded into spherical harmonics [19, 20] and used for integrals as in (5) and (10). The single-scattering solutions R_L^n and S_L^n were calculated by first solving the radial Schrödinger equation for the spherical part of the potential and then iterating a Born series (up to fourth order) to include the non-spherical part as described in [8, 21]. The numerical investigations were done for the technologically important semiconductor GaN. Instead of the more complicated wurtzite structure the zinc-blende structure (with the experimental lattice constant $a = 0.452$ nm [22]) was used. To avoid too elongated cells around the atoms, the zinc-blende structure was treated as a face-centred-cubic lattice with four basis sites along the (111) direction. Two sites were occupied by Ga and N atoms and two sites were empty.

The potential for GaN was determined self-consistently according to the local-density approximation (LDA) [23]. The single-scattering solutions R_L and S_L were used up to $l_{\max} = 3$ and density and potential were expanded into multipoles up to $2l_{\max} = 6$. The 2s states for N and the 3d states for Ga were included in the valence states and the deeper states were treated as atomic core states. The density for the valence states was evaluated by contour integration [24, 25] with 74 complex energy points adapted to a finite temperature $T = 800$ K. For the Brillouin-zone integration 8555 uniformly distributed $\mathbf{k}$ points were used in 1/24th of the zone. The screened structure constants $G_{LL'}^{r,\nu\nu'}(\mathbf{k}, E)$ were determined with clusters in real space, consisting of 169 repulsive muffin-tin potentials of height 8 Ryd in the appropriate body-centred-cubic arrangement. If not stated otherwise, all calculations presented below were also done with $l_{\max} = 3$ and with 169 repulsive potentials to determine the screened structure constants. The potential constructed in this way leads to a bandgap of 1.99 eV, which is smaller than the experimental value (3.2 eV [22]). The difference between the calculated and the experimental bandgap, which is caused by the LDA and the discontinuity of the exchange–correlation potential, represents no problem for the present study, since here the LDA calculation is only used to provide an illustrative example. It should be noted that the particular choice of the potential is not important for the present investigation. Any reasonable potential would give qualitatively similar results and would not change the conclusions.

4. Angular-momentum convergence

The potential constructed as described above was applied to calculate the number of states as a function of the chemical potential μ according to (1) using the Green-function representation (2) and according to (6) using Lloyd's formula (8). In figure 1 the results obtained by the $T = 0$ limit of (6), which is given by $N_e(\mu, 0) = \operatorname{Im} N(\mu)$, and by extrapolating (1) to $T = 0$ are shown for $l_{\max} = 2$, 3, 4 and 6. Here $l_{\max}$ was taken to be the same for

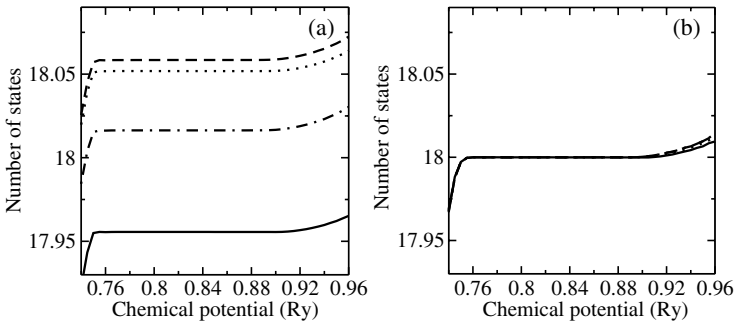

Figure 1. Number of states for GaN as a function of the chemical potential, (a) calculated by the Green-function representation (2) and (b) calculated by Lloyd's formula (8). The results for $l_{\max} = 2$, 3, 4, and 6 are given by the solid, dotted, dashed, and dot–dashed curves. 8555 **k** points were used in 1/24th of the Brillouin zone and 65 repulsive potentials were used to determine the screened structure constants.

the single-scattering solution R_L and S_L, for the $\Delta t_{LL'}$ and $\Delta\alpha_{LL'}$ matrices, for the Green-function matrix elements $G^{nn'}_{LL'}$ and for the sums in (2). Figure 1 clearly shows that the results calculated by Lloyd's formula converge much better with $l_{\max}$ than the results calculated by the Green-function representation (2). The results obtained by (2) also considerably deviate from the exact result 18, which is obtained by counting the 13 valence states of Ga and the five valence states of N. For instance, near the middle of the gap (at $\mu = 0.825$ Ryd), the truncation of (2) leads to errors of -0.044, 0.052, 0.058 and 0.016 for $l_{\max} = 2$, 3, 4 and 6, whereas the error of Lloyd's formula is always less than 0.000 05 independent of $l_{\max}$. Thus, if the Fermi level is calculated from the Green function by L summation, the results in figure 1(a) show that the Fermi level falls into the conduction band for $l_{\max} = 2$ and into the valence band for $l_{\max} = 3$, 4 and 6.

The good convergence of Lloyd's formula (8) is a consequence of the fact that for higher angular momenta the single-scattering solutions R_L and S_L usually rapidly converge to the corresponding free-space solutions. If changes for $l > l_{\max}$ are neglected, the t and α matrices can be written in block form as

$$t = \begin{bmatrix} \tilde{t} & 0 \\ 0 & 0 \end{bmatrix} \qquad \text{and} \qquad \alpha = \begin{bmatrix} \tilde{\alpha} & 0 \\ 0 & 1 \end{bmatrix} \tag{11}$$

with $\det\alpha = \det\tilde{\alpha}$. Here the matrices $\tilde{t}$ and $\tilde{\alpha}$ have finite dimension $(l_{\max} + 1)^2$. The approximation (11) enables us to evaluate Lloyd's formula from matrices of finite dimension without any further angular-momentum truncation. In particular, the result depends only on Green-function matrix elements $G^{r,nn'}_{LL'}$ or $G^{r,\nu\nu'}_{LL'}$ with $l, l' \leqslant l_{\max}$, whereas the Green-function representation (2) depends on all elements $G^{nn'}_{LL'}$ even if the approximation (11) is used. Thus (2) requires an additional truncation of the angular-momentum sums, which is the reason for the much slower convergence seen in figure 1(a). The approximation (11) can be understood as a replacement of the potential by a projection potential, which acts only on the lower angular momenta $l \leqslant l_{\max}$. This replacement slightly modifies the position and size of the gap and also slightly affects the calculated number of states in the energy region of the valence and conduction bands, but does not change the exact integer number of states in the gap region. This means that, independent of $l_{\max}$, Lloyd's formula (8) always gives the exact result for the number of states in the gap, whereas an exact result cannot be obtained from (2), since the truncation of the sums always causes a systematic error because the correct number of states in the gap is only obtained in the limit $l_{\max} \to \infty$.

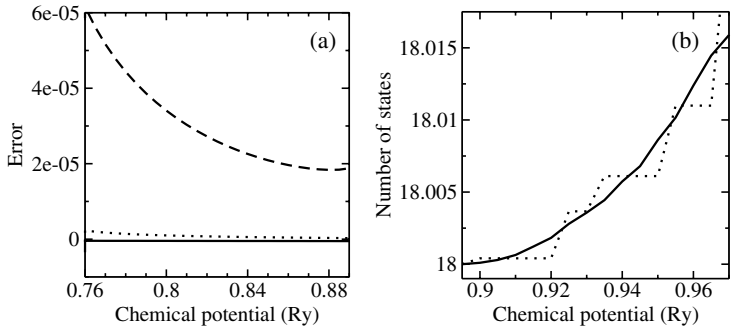

Figure 2. (a) Error of the number of states in the gap and (b) number of states at the bottom of the conduction band. The results on the left were calculated with 8555 **k** points in 1/24th of the Brillouin zone and with screened structure constants obtained from 387, 169 and 65 repulsive potentials (solid, dotted and dashed curves). The results on the right were calculated with 169 potentials and 8555 and 285 **k** points (solid and dotted curves). Lloyd's formula was used for $N_e(\mu, 0) = \mathrm{Im}\, N(\mu)$, the zero-temperature limit of (6).

5. Dependence on k integration and screened structure constants

From the good angular-momentum convergence shown in figure 1(b) it can be expected that the accuracy of Lloyd's formula depends on the number of **k** points used for the Brillouin-zone sampling and on the number of repulsive potentials used for the real-space determination of the screened structure constants in a similar way for different values of $l_{\max}$. This expectation was confirmed by test calculations and only results for $l_{\max} = 3$ are presented here. It was found that the number of **k** points and the number of repulsive potentials have quite different effects on the results in the gap and in the valence and conduction bands. This is illustrated in figure 2, where the left part concentrates on the gap and the right part on the bottom of the conduction band. The behaviour in the valence band, not shown, is very similar to the behaviour in the conduction band, although the errors are less visible because the number of states changes more rapidly at the top of the valence band than at the bottom of the conduction band.

In the gap the deviations from the exact result 18 are very small, less than 2×10^{-6} if 169 repulsive potentials are used, and less than 0.5×10^{-6} if 387 repulsive potentials are used, and the results are well converged with the number of **k** points. For instance, calculations with 285 instead of 8555 **k** points lead to curves, which cannot be distinguished on the scale of figure 2(a). It should be emphasized here that the good **k** convergence in the gap, which one naively expects for semiconductors, critically depends on the choice of the reference system. For the usual choice of a free-space reference system the integrated density of states has a metallic $E^{3/2}$ behaviour. For this choice the Brillouin-zone integration in (8) is always as complicated as in metallic systems, since (8) contains the difference between a semiconducting and a metallic system. The repulsive reference system chosen here has no eigenstates below a positive energy E_{bot}, which in first-order perturbation theory is approximately given by the product of the potential height and the volume fraction covered by the muffin-tin spheres. In the repulsive system $\mathrm{Im}\, N^r(E)$ vanishes for $E < E_{\mathrm{bot}}$ and in the gap the Brillouin-zone integration is simple and fast converging as in semiconductors.

In the conduction band the results in figure 2(b) show deviations from the expected smooth behaviour, which are much larger than the errors in the gap. The curve calculated with 285 **k** points has flat regions and the curve calculated with 8555 **k** points has small kinks. These unrealistic features arise from a poor **k** convergence of the Brillouin-zone sampling due to the

metallic character of the band structure in the conduction band. Changes arising from different numbers (65, 169 or 387) of repulsive potentials are small and cannot be distinguished on the scale of figure 2(b). The main reason for the poor **k** convergence is the phase problem discussed in section 1.

For the results in figure 2 the phase of the logarithm of the KKR determinant $\ln\det|1 - G(\mathbf{k}, E)\Delta t(E)|$ was determined by an extrapolation method, which is routinely applied in calculations for impurities [5]. This method uses a complex energy contour, which begins on the real energy axis above the core states and below the valence states and ends at the Fermi level. If the mesh points on the contour are close enough, for each value of **k** the phase can be estimated at a mesh point by extrapolation from the phases already known at two previous mesh points. This estimate can be used to add the proper multiple of 2π to the imaginary part of the logarithm of the KKR determinant and to find the correct phase of the logarithm. At the beginning of the contour the phase is known from Levinson's theorem by counting the number of core states. The extrapolation works quite well in the bandgap, but is not so good for the conduction and valence bands. Here, with the 74 mesh points used on the contour, the extrapolation seems to fail for some **k** points and only an average over many **k** points leads to reasonable results. The results could be improved by using more mesh points on the contour, but then the calculations are very expensive. Therefore the question of whether finite electronic temperatures can help to reduce the numerical effort is an important issue. This will be investigated in the next section.

6. Finite temperatures

Finite electronic temperatures connected with fractional occupation numbers are often used in density-functional calculations in order to reduce the number of **k** points in the Brillouin zone and are of particular importance for Green-function multiple-scattering calculations [25–27]. It is therefore interesting to investigate how finite temperatures can help in applications of Lloyd's formula. The correct temperature dependence of $N_e(\mu, T)$ arising from the Fermi–Dirac statistics can be obtained if the integral in (6) is evaluated carefully. Note that as usual in Green-function methods the integral is defined for complex energies and understood in the limit $\operatorname{Im} E \to +0$. Instead of integrating (6) for real energies, where the Green function has poles and branchcuts arising from core and band states, it is numerically easier to use contour integrals in the complex plane to take advantage of the smoother behaviour of the Green function away from the real axis. At complex energies the only singularities in (6) come from the second order poles of the derivative of the Fermi–Dirac function at the Matsubara frequencies $E_n = \mu + (2n + 1)\mathrm{i}\pi kT$ for $n \in \mathbb{Z}$. The contour integration was tested for two contours C_1 and C_2, which are both parallel to the real axis with distances $\operatorname{Im} E = \pi kT/2$ and $\operatorname{Im} E = 2\pi kT$. These contours were chosen because the simple form of the Fermi–Dirac function on C_1 and C_2 allows for an easy construction of numerical integration rules as explained in the appendix. Contour C_1 has the advantage that it avoids the singularities of the Fermi–Dirac function, but it is rather near to the real axis. Contour C_2 has a four times larger distance from the real axis, but the contribution of a Matsubara pole must be evaluated from the derivative $\operatorname{Im} N'(\mu + \mathrm{i}\pi kT)$, which was obtained by numerical differentiation as explained in the appendix. For the contour integrals Gaussian integration rules

$$-\operatorname{Im}\int_C \mathrm{d}E\, N(E)\frac{\mathrm{d}}{\mathrm{d}E} f(E, \mu, T) \approx \sum_{j=1}^{J} \operatorname{Im}(w_j N(E_j)), \tag{12}$$

for low order J were found to be sufficient. By change of variable the mesh points can be expressed as $E_j = \mu + kTx_j$ and the weight function $-\frac{\mathrm{d}}{\mathrm{d}E} f(E, \mu, T)$ as $w_1(x) =$

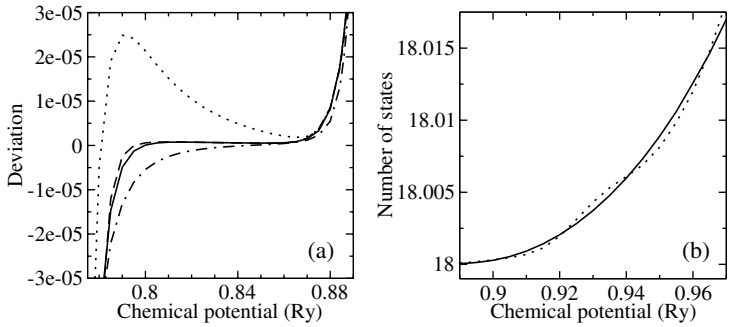

Figure 3. For $T = 800$ K: (a) in the gap deviation of the number of states from the exact midgap value 18 and (b) number of states at the bottom of the conduction band. The results on the left, which are again well converged with the number of **k** points, were calculated with 8555 **k** points. The dash–dotted and dashed curves are for contour C_1 with $J = 2$ and 4 and the dotted and solid curves are for contour C_2 with $J = 2$ and 4. The solid curve is also obtained for contour C_1 with $J = 6$. The results on the right were calculated with 8555 and 285 **k** points (solid and dotted curves) for contour C_1 with $J = 2$.

Table 1. Mesh points and weights for Gaussian integration over infinite intervals on contour C_1 and C_2 with the weight functions $w_1(x)$ and $w_1(x)$ given in the text. The first two lines are for order $J = 2$ and the last four lines for order $J = 4$. Only the positive mesh points are listed; the negative ones are given by $-x_j$ with complex conjugate weights $\overline{w}_j$.

	For Im N on C_1	For Re N on C_1	For Im N on C_2
x_1	$0.288\,675\,1346\pi$	$0.866\,025\,4038\pi$	$0.577\,350\,2692\pi$
w_1	0.500 000 0000	−0.288 675 1346i	0.500 000 0000
x_1	$0.934\,540\,6979\pi$	$2.232\,950\,5094\pi$	$1.869\,081\,3959\pi$
x_2	$0.234\,957\,6823\pi$	$0.716\,890\,5234\pi$	$0.469\,915\,3646\pi$
w_1	0.017 189 9014	−0.005 909 9389i	0.017 189 9014
w_2	0.482 810 0986	−0.330 320 1691i	0.482 810 0986

$\frac{1}{4}\cos h^{-2}(x/2 + \mathrm{i}\pi/4)$ for contour C_1 and as $w_2(x) = \frac{1}{4}\cos h^{-2}(x/2)$ for contour C_2. For contour C_2 the weight function is real and positive and only the imaginary part of $N(E)$ contributes. For contour C_1 the weight function is complex with a positive real part and an imaginary part, which changes sign at $x = 0$, and both the real and imaginary part of $N(E)$ contribute. For the low order integration rules used here, it was found that the non-positivity did not prevent us obtaining accurate results. Values for x_j and for the weights w_j, which were obtained as described in the appendix, are given in table 1.

It turned out that $J = 2$ already leads to very satisfactory results as can be seen in figure 3. On the other hand, $J = 1$ with mesh point $x_1 = 0$ and weights $w_1 = 1$ for Im $N(E)$ and $w_1 = 0$ for Re $N(E)$ is not adequate, since $J = 1$ just gives a Lorentzian broadening with unacceptable long tails, which immediately spoil the bandgap. In the gap, for both contours, the results show good convergence with the order of the integration rule, with errors smaller than 3×10^{-5} for $J = 2$. Fully converged results were obtained with $J = 4$ for contour C_2 and with $J = 6$ for contour C_1. The larger difference of the $J = 2$ curve for C_2 can be explained by the larger difference of the mesh points on the C_2 and the better convergence on C_2 can be explained by its larger distance from the real energy axis with the connected smaller variations of $N(E)$ in (6). The results in figure 3(a) are also insensitive to the formula used for the numerical differentiation to obtain the Matsubara pole contribution. The results obtained by the two-point formula (A.9) or by the four-point formula (A.10) differed less than 10^{-6}.

In the conduction band the comparison of the results for $T = 800$ K in figure 3(b) with the results for $T = 0$ K in figure 2(b) shows that the use of finite temperatures leads to considerably better results. The curve calculated with 8555 **k** points has the expected smooth behaviour and also the slightly wavy curve calculated with 285 **k** points is much better than the unrealistic one in figure 2(b). For $T = 2000$ K the difference between calculations with 285 or 8555 **k** points is even more reduced. This indicates that finite temperatures can help to simplify the phase determination in the extrapolation method. Nevertheless, it was found that for $J = 4$ the relatively large distances between the mesh points on the contours sometimes produced failures of the extrapolation and prevented us obtaining consistently smooth curves in valence and conduction bands. Only $J = 2$ produced smooth curves, which agreed very well for both contours. Presumably, with additional extrapolation points on the contours the failures could be avoided. This was not investigated, since the method presented in the next section turned out to be much more advantageous, if Lloyd's formula is used together with finite temperatures.

7. Solution for the phase problem

The smooth dependence of Lloyd's formula as a function of complex energy, which was the reason for the stability of the results in the previous section with respect to numerical integration and differentiation, can be exploited to replace the cumbersome extrapolation method for the determination of the phase of the complex logarithm by an alternative. The alternative is based on the observation that the numerical derivative of Lloyd's formula can accurately be calculated already by the simple formula (A.9). The alternative consists in partially integrating (6) as

$$N_e(\mu, T) = \mathrm{Im} \int_{-\infty}^{\infty} \mathrm{d}E\, f(E, \mu, T) \frac{\mathrm{d}}{\mathrm{d}E} N(E) \tag{13}$$

and in evaluating the derivative in (13) numerically. For the derivative $\frac{\mathrm{d}}{\mathrm{d}E} N(E)$ it is important to note that any analytical function $f(z) = u(z) + \mathrm{i}v(z)$ of the complex variable $z = x + \mathrm{i}y$ with real $u(z)$ and $v(z)$ satisfies the Riemann–Cauchy conditions, which are given by $\frac{\mathrm{d}u}{\mathrm{d}x} = \frac{\mathrm{d}v}{\mathrm{d}y}$ and $\frac{\mathrm{d}u}{\mathrm{d}y} = -\frac{\mathrm{d}v}{\mathrm{d}x}$. This means that the derivative in (13) can be evaluated from the real part $\mathrm{Re}\, N(E)$ alone by calculating its derivative in the directions parallel and perpendicular to the real axis with the result

$$\frac{\mathrm{d}N(E)}{\mathrm{d}E} = \frac{\mathrm{dRe}\, N(E)}{\mathrm{dRe}\, E} - \mathrm{i} \frac{\mathrm{dRe}\, N(E)}{\mathrm{dIm}\, E}. \tag{14}$$

Since the real part of $N(E)$ only depends on the single-valued real part of the complex logarithm, the difficulty with the multivalued imaginary part of the logarithm is completely avoided in the derivative (14). Since the integral (13) is in one-to-one correspondence to the integral

$$n(\mathbf{r}, T) = -\frac{1}{\pi} \mathrm{Im} \int_{-\infty}^{\infty} \mathrm{d}E\, f(E, \mu, T) G(\mathbf{r}, \mathbf{r}, E) \tag{15}$$

for the charge density, the same contours and mesh points can be used to calculate the number of states and the charge density simultaneously. As already expected from the results in section 6 the numerical differentiation of (14) was found to be insensitive to the choice of formula (A.9) or (A.10) with differences smaller than 10^{-6} and to be stable with respect to the step size h. For 8555 **k** points the results calculated by use of (14) completely agreed with the solid curves in figure 3 and for fewer **k** points the expected smooth behaviour for the number of states was always found. It is important to note that the differentiation method presented here can also considerably reduce the effort in the Brillouin-zone sampling. Whereas the extrapolation must be done separately for each **k** point and thus requires the same high number of **k** points at all

Table 2. Fit parameters $a_v(T)$ and $a_c(T)$ and Fermi level $\mu_0 = E_F(T)$.

T (K)	400	800	1200	1600	2000
a_v	0.003 754	0.011 12	0.020 82	0.032 72	0.046 81
a_c	0.000 062 90	0.000 1844	0.000 3664	0.000 6106	0.000 9250
μ_0 (Ryd)	0.829 130	0.834 336	0.839 303	0.844 123	0.848 804

energy mesh points, the differentiation method requires a high number of **k** points only at the Matsubara frequencies $E_n = \mu + (2n+1)\mathrm{i}\pi kT$ nearest to μ. This was checked and it turned out that 91 **k** points were enough to give results with an accuracy of about 10^{-6} provided that the number of **k** points was increased at E_0 and E_1 to 8555 and 506 and at E_2 and E_3 to 285. Thus (14) together with (13) opens the way to an efficient and accurate calculation of total number of states by avoiding the problem of the multivalued imaginary part of $N(E)$.

8. Temperature dependence of the Fermi level

The high accuracy and the reliability of the method presented in the previous section is illustrated here by applying Lloyd's formula to a numerically difficult problem, which is the determination of the influence of the Fermi–Dirac statistics on the temperature dependence of the intrinsic Fermi level in GaN. The textbook result for the Fermi level

$$E_F(T) = \frac{1}{2}(E_v + E_c) + \frac{3}{4}kT \ln\left(\frac{m_v}{m_c}\right) \tag{16}$$

is derived under the conditions that the temperature is small compared to the gap ($kT \ll E_c - E_v$) and that the relevant bands are parabolically shaped. The effective masses m_v and m_c at the valence band maximum E_v and conduction band minimum E_c are difficult to calculate. They are usually determined by fitting the bands obtained by density-functional calculations to model Hamiltonians of Kohn–Luttinger or $\mathbf{k}\cdot\mathbf{p}$ type. This works for GaN with its bandgap at the Γ point, but becomes extremely complicated for semiconductors consisting of more elements or occurring in less symmetric structures. An expensive method, which avoids the detailed knowledge of the band structure, is the accurate calculation of the densities of states near E_v and E_c by straightforward Brillouin-zone integrations with unbiased **k** point meshes and the use of these densities of states in integrals as (1) or (13).

The disadvantage of the use of effective masses or accurate densities of states near E_v and E_c is that their calculation is not simplified by the temperature broadening, which is only afterwards applied in the integrals (1) or (13). On the other hand, the temperature is directly included, if the integrals are evaluated along complex energy contours as described in sections 6 and 7. The calculated results for the temperature dependence of the number of states were accurate enough to determine the Fermi level $\mu_0 = E_F(T)$ from the solution of $N_e(\mu_0, T) = 18$. For large temperatures ($T \gtrsim 2000$ K) this solution could be obtained directly, whereas for smaller temperatures the differences between $N_e(\mu, T)$ and 18 were too small in the vicinity of μ_0 because of the exponential temperature dependence. Then μ_0 could be obtained from the global behaviour of $N_e(\mu, T) - 18$ as a function of μ. It was found that this function could well be fitted for μ values between the calculated band edges $E_v = 0.751\,17$ Ryd and $E_c = 0.896\,73$ Ryd by two exponentials $N_c(T) = a_c \exp(-\beta(E_c - \mu))$ and $N_v(T) = a_v \exp(-\beta(\mu - E_v))$ for the numbers of occupied conduction and unoccupied valence states. The condition $N_c(T) = N_v(T)$ with the solution $\mu_0 = \frac{1}{2}(E_v + E_c) + \frac{1}{2}b^{-1}\ln(a_v/a_c)$ then determines the Fermi level, which is given in table 2 together with the calculated fit parameters a_c and a_v for several temperatures. As a function of temperature the calculated

Fermi level is well described by $E_F(T) = 0.8244\,\text{Ryd} + 1.939kT$ or even better by $E_F(T) = 0.8238\,\text{Ryd} + 2.142kT - 13.3k^2T^2$. The close agreement between the extrapolated zero-temperature values 0.8244 and 0.8238 Ryd and the result $\frac{1}{2}(E_v + E_c) = 0.823\,95$ Ryd, which was obtained directly from band-structure calculation for real energies, is a consequence of the accuracy of the calculated Fermi levels in table 2. This shows that even with a moderate number of **k** points Lloyd's formula used with finite-temperature contour integrals allows for very accurate calculations of the number of states.

9. Summary

The angular-momentum convergence of Lloyd's formula was found to be much faster than the convergence of the multiple-scattering Green function, particularly in the gap of semiconductors or insulators, where Lloyd's formula always gives the exact result independent of the angular-momentum cut-off. This was explained by the fact that the calculation of the Green function requires a truncation of slowly converging angular-momentum sums, whereas the calculation of Lloyd's formula only requires us to omit angular-momentum channels with rapidly decreasing contributions. The omission changes the potential into a projection potential, which slightly changes the band edges, but not the exact integer number of states in the gap. It was pointed out that in the gap the choice of a repulsive reference system as used in the tight-binding KKR method leads to fast converging Brillouin-zone samplings, which cannot be achieved by the usual free-space reference system because of its metallic character.

It was shown that Lloyd's formula can be used at finite temperatures with the physically correct Fermi–Dirac behaviour by exploiting contour integrals in the complex energy plane and that Lloyd's formula could be accurately numerically differentiated for complex energies. This fact together with the Riemann–Cauchy conditions for analytical functions enabled us to develop a method which avoids the difficult determination of correct phases of multivalued imaginary parts of complex logarithms, since it works with single-valued real parts alone. It was shown that this method, which uses complex energy integration contours in one-to-one correspondence to the ones used for charge-density calculations, is reliable and accurate enough to determine the influence of the Fermi–Dirac statistics on the temperature dependence of the intrinsic Fermi level in semiconductors. From the experience with impurity calculations it is also expected that this reliable and accurate method for Lloyd's formula leads to improved total energies in the KKR Green-function method for bulk and surface systems.

In principle, the one-to-one correspondence, which is valid for each energy (and at each **k** point), could be used to normalize the charge density calculated with an l_{max} cut-off by the number of states calculated with Lloyd's formula. This would enable a consistent determination of charge density and Fermi level, but since the real part of (2) summed over all L diverges for $\mathbf{r}' = \mathbf{r}$ further investigations are necessary, which are planned for the future.

Acknowledgment

It is my pleasure to thank Professor P H Dederichs for his continued interest in this work and for many helpful and constructive suggestions and discussions.

Appendix. Integration and differentiation rules

The mesh points E_j and the weights w_j for the integration rule (12) were determined by the condition that the exact result is obtained if $N(E)$ is a polynomial in E of order $2J - 1$ or less.

Table A.1. Moments M_2 to M_7 defined by (A.2).

a	M_2	M_3	M_4	M_5	M_6	M_7
1	$\pi^2/3$	0	$7\pi^4/15$	0	$31\pi^6/21$	0
i	$\pi^2/12$	$-3\mathrm{i}\pi^3/8$	$7\pi^4/240$	$-25\mathrm{i}\pi^5/32$	$31\pi^6/1344$	$-427\pi^7/128$

This condition, which leads to a set of non-linear equations for E_j and w_j, can be written as

$$M_n = \sum_{j=1}^{J} w_j E_j^n \qquad \text{with } n = 0, 1, 2, \ldots 2J-1, \tag{A.1}$$

where M_n denote the moments of the weight function $-\frac{\mathrm{d}}{\mathrm{d}E} f(E, \mu, T)$, which are defined as

$$M_n(a) = -\int_{-\infty}^{\infty} \mathrm{d}x\, x^n \frac{\mathrm{d}}{\mathrm{d}x} \frac{1}{1 + a\exp(x)}. \tag{A.2}$$

Here the parameter a is equal to i for contour C_1 and equal to unity for contour C_2. The integral in (A.2) can be evaluated analytically. By the use of two intervals from $-\infty$ to 0 and from 0 to ∞ and with the substitution $-x$ for x in the first interval, the moments are given by

$$M_n(a) = (-1)^n \int_0^{\infty} \mathrm{d}x\, x^n \frac{\mathrm{d}}{\mathrm{d}x} \frac{1}{1 + a\exp(-x)} - \int_0^{\infty} \mathrm{d}x\, x^n \frac{\mathrm{d}}{\mathrm{d}x} \frac{1}{1 + a\exp(x)}. \tag{A.3}$$

This can be expressed in the form $M_n(a) = (-1)^n I_n(a) + I_n(a^{-1})$ by use of

$$\frac{1}{1 + a\exp(-x)} = 1 - \frac{a\exp(-x)}{1 + a\exp(-x)}, \tag{A.4}$$

$$\frac{1}{1 + a\exp(x)} = \frac{a^{-1}\exp(-x)}{1 + a^{-1}\exp(-x)} \tag{A.5}$$

and

$$I_n(a) = -\int_0^{\infty} \mathrm{d}x\, x^n \frac{\mathrm{d}}{\mathrm{d}x} \frac{a\exp(-x)}{1 + a\exp(-x)}. \tag{A.6}$$

For $n = 0$ the integration in (A.6) is trivial and gives $I_0(a) = a(1+a)^{-1}$ and $M_0(a) = 1$. For $n \neq 0$ partial integration yields

$$I_n(a) = n\int_0^{\infty} \mathrm{d}x\, x^{n-1} \frac{a\exp(-x)}{1 + a\exp(-x)}. \tag{A.7}$$

Here for $n = 1$ the substitution $y = \exp(-x)$ leads to an elementary integral with the result $I_1(a) = \ln(1+a)$, which leads to $M_1(1) = 0$ and $M_1(\mathrm{i}) = -\mathrm{i}\pi/2$. For $n > 1$ the denominator in (A.7) can be expanded into a geometric series as proposed by Sommerfeld [28]. The result

$$I_n(a) = -n\int_0^{\infty} \mathrm{d}x\, x^{n-1} \sum_{k=1}^{\infty} (-a)^k \exp(-kx) = -\Gamma(n+1) \sum_{k=1}^{\infty} (-a)^k k^{-n} \tag{A.8}$$

can be written in terms of Riemann's zeta function if $a = 1$, and in terms of polylogarithms if $a = \mathrm{i}$. Explicit results for the moments M_2 to M_7, which together with M_0 and M_1 given above are necessary to derive rules up to order $J = 4$, are listed in table A.1.

The derivative $\mathrm{Im}\, N'(\mu + \mathrm{i}\pi kT)$ was obtained by numerical differentiation either from the symmetric two-point formula

$$N'(E) = \frac{1}{2h}[N(E+h) - N(E-h)] \tag{A.9}$$

or from the symmetric four-point formula

$$N'(E) = \frac{1}{12h}[8N(E+h) - 8N(E-h) - N(E+2h) + N(E-2h)] \tag{A.10}$$

with the step size chosen as $h = \pi kT/100$. It was found that the results for $N'(E)$ practically do not depend on h, even if it is increased or decreased by a factor of ten.

References

[1] Lloyd P 1967 *Proc. Phys. Soc. London* **90** 207
[2] Lloyd P and Smith P V 1972 *Adv. Phys.* **21** 69
[3] Korringa J 1947 *Physica* **13** 392
[4] Kohn W and Rostoker N 1954 *Phys. Rev.* **94** 1111
[5] Drittler B, Weinert M, Zeller R and Dederichs P H 1989 *Phys. Rev.* B **39** 930
[6] Zeller R, Dederichs P H, Újfalussy B, Szunyogh L and Weinberger P 1995 *Phys. Rev.* B **52** 8807
[7] Zeller R 2004 *J. Phys.: Condens. Matter* **16** 6453
[8] Papanikolaou N, Zeller R and Dederichs P H 2002 *J. Phys.: Condens. Matter* **14** 2799
[9] Treusch J and Sandrock R 1966 *Phys. Status Solidi* **16** 487
[10] Kaprzyk S and Barnsful A 1990 *Phys. Rev.* B **42** 7358
[11] Zhang X-G and Butler W H 1992 *Phys. Rev.* B **46** 7433
[12] Tatarchenko A F and Kulikov N 1994 *Phys. Rev.* B **50** 8266
[13] Kaprzyk S 1997 *Acta Phys. Pol.* A **91** 135
[14] Moghadam N Y, Stocks G M, Zhang X-G, Nicholson D M C, Shelton W A, Wang Y and Faulkner J S 2001 *J. Phys.: Condens. Matter* **13** 3073
[15] Lehmann G 1975 *Phys. Status Solidi* b **70** 737
[16] Drittler B 1991 *Dissertation* Rheinisch-Westfälische Technische Hochschule Aachen
[17] Dederichs P H, Drittler B and Zeller R 1992 *Application of Multiple Scattering Theory to Materials Science* (*MRS Symp. Proc. No. 253*) ed W H Butler, P H Dederichs, A Gonis and R L Weaver (Pittsburgh, PA: Materials Research Society) p 185
[18] Ham F S and Segall B 1961 *Phys. Rev.* **124** 1786
[19] Stefanou N, Akai H and Zeller R 1990 *Comput. Phys. Commun.* **60** 231
[20] Stefanou N and Zeller R 1991 *J. Phys.: Condens. Matter* **3** 7599
[21] Drittler B, Weinert M, Zeller R and Dederichs P H 1991 *Solid State Commun.* **79** 31
[22] Lei T, Moustakis T D, Graham R J, He Y and Berkowitz S J 1992 *J. Appl. Phys.* **71** 4933
[23] Vosko S H, Wilk L and Nusair M 1980 *Can. J. Phys.* **58** 1200
[24] Zeller R, Deutz J and Dederichs P H 1982 *Solid State Commun.* **44** 993
[25] Wildberger K, Lang P, Zeller R and Dederichs P H 1995 *Phys. Rev.* B **52** 11502
[26] Nicholson D M C, Stocks G M, Wang Y, Shelton W A, Szotek Z and Temmerman W M 1994 *Phys. Rev.* B **50** 14686
[27] Nicholson D M C and Zhang X-G 1997 *Phys. Rev.* B **56** 12805
[28] Sommerfeld A 1928 *Z. Phys.* **47** 1